Electronic Supplementary Information

Electrochemical Elucidation of $Co_{0.5}M_{0.5}V_2O_4$ (M = Fe or Zn) Nanocomposite Anode Materials for Li-Ion Storage

Rasu Muruganantham,[a] Jeng-Shin Lu,[a] Bor Kae Chang,[b] Po Kai Wang,[b] and Wei-Ren Liu*[a]

[a] Department of Chemical Engineering, R&D Center for Membrane Technology,
Research Center for Circular Economy, Chung Yuan Christian University, Taoyuan City 32023, Taiwan, Republic of China
[b] Department of Chemical and Materials Engineering, National Central University,
No. 300, Jhongda Rd., Chung Li District, Taoyuan City 32001, Taiwan, Republic of China.

*Correspondence: WRLiu1203@gmail.com, wrliu@cycu.edu.tw
Tel: +886-3-2654140; Fax: +886-3-2654199

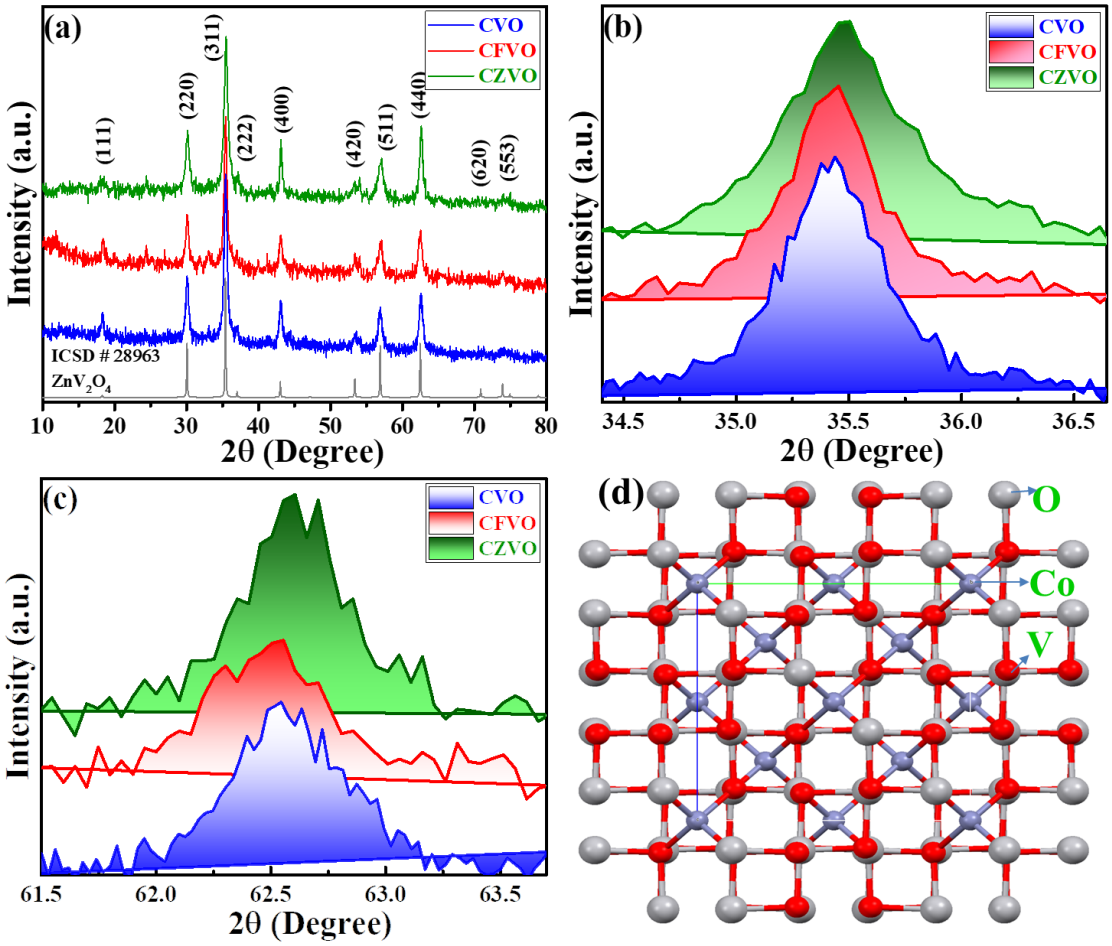

Fig. S1. XRD patterns of the as-prepared bare CoV_2O_4, $Co_{0.5}Fe_{0.5}V_2O_4$ and $Co_{0.5}Zn_{0.5}V_2O_4$ **(a)** full-range 2θ=10-80°, **(b, c)** enlarged 2θ=34.4-36.6° & 2θ=61.5-63.7°, and **(d)** schematic molecule packing *'a'* axis view of CoV_2O_4 cubic spinel structure.

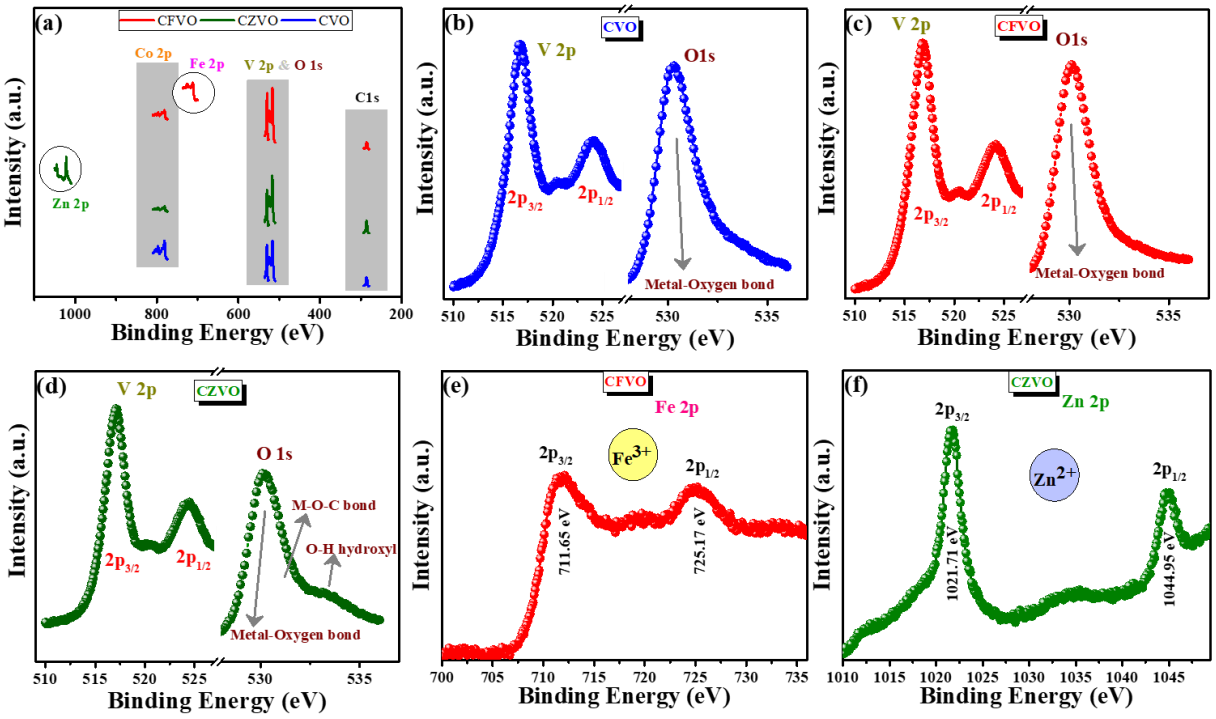

Fig. S2. X-ray photoelectron spectroscopy (XPS) of **(a)** comparable view of presences of elements in the wide-range spectra; **(b-d)** V 2p and O 1s nano-scan core spectra of CoV_2O_4, $Co_{0.5}Fe_{0.5}V_2O_4$ and $Co_{0.5}Zn_{0.5}V_2O_4$ materials; **(e)** nano-scan Fe 2p spectrum in $Co_{0.5}Fe_{0.5}V_2O_4$; and **(f)** nano-scan Zn 2p spectrum in $Co_{0.5}Zn_{0.5}V_2O_4$ samples.

Table S1. The Co 2p X-ray photoelectron spectra binding energy and the ratio of Co^{2+}/Co^{3+} in the prepared samples.

Samples	**Co^{2+}** (eV)	**Co^{3+}** (eV)	**Co^{2+}/Co^{3+}** (eV)
CVO	3040.5	1285.4	2.4
CFVO	945.7	1002.3	0.9
CZVO	714.3	275.9	2.6

Table S2. The observed binding energy of V, O, Fe, Zn elements from XPS spectra of the prepared samples.

Elements	CVO (eV)	CZVO (eV)	CFVO (eV)
V 2p $2p_{3/2}$ $2p_{1/2}$	516.7 520.5 524.1	517.1 520.6 524.3	516.8 520.4 524.2
O 1s	530.3 532.1	530.3 531.9 533.2	530.1 531.5 533.3
Fe 2p $2p_{3/2}$ $2p_{3/2}$	-	-	711.7 725.2
Zn 2p $2p_{3/2}$ $2p_{1/2}$	-	1021.7 1044.9	-

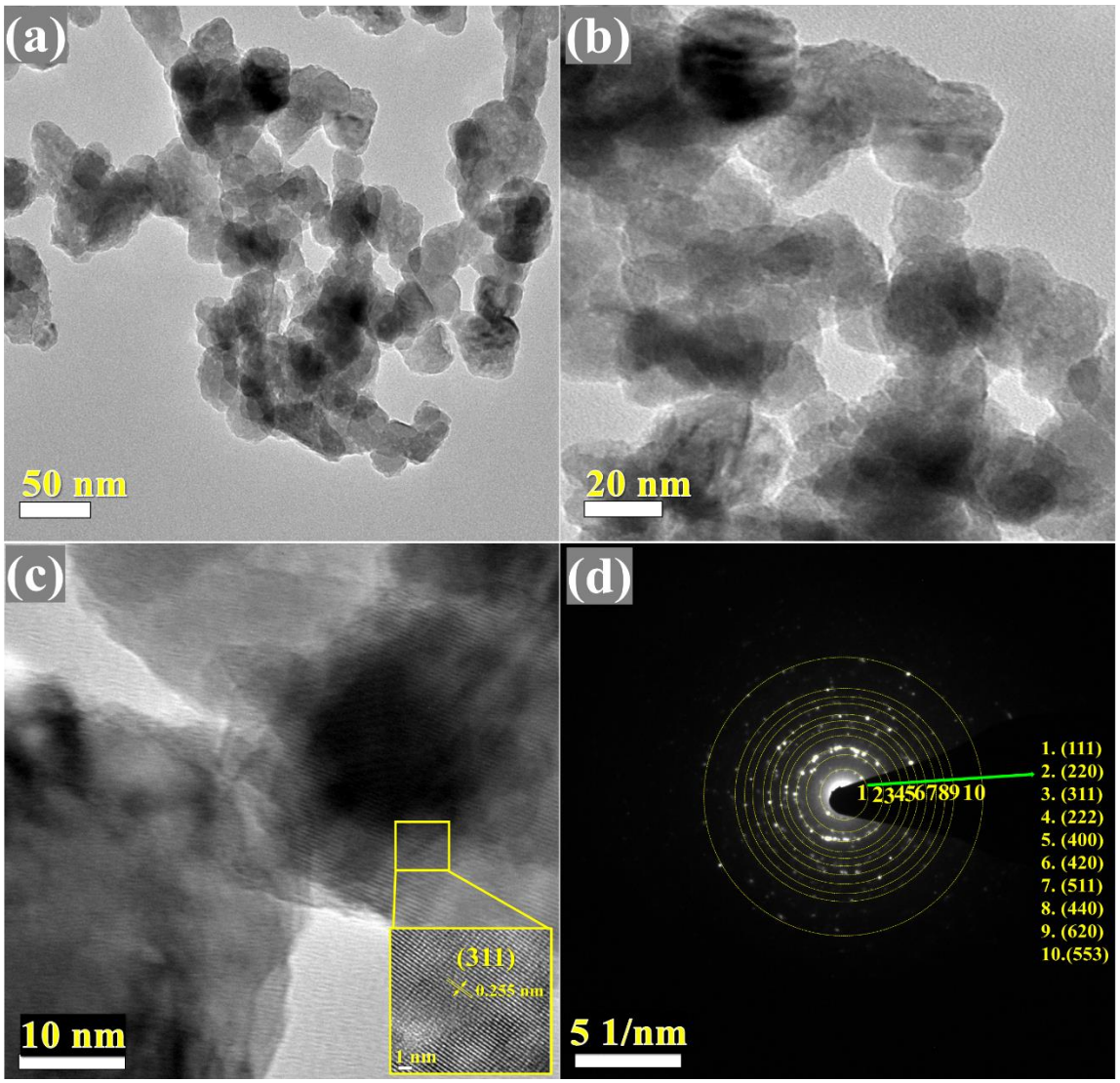

Fig. S3. (a-c) Different magnification HR-TEM images and **(d)** SAED of CVO sample. The inset of Fig.S3(c) represents the enlarged view of lattice image.

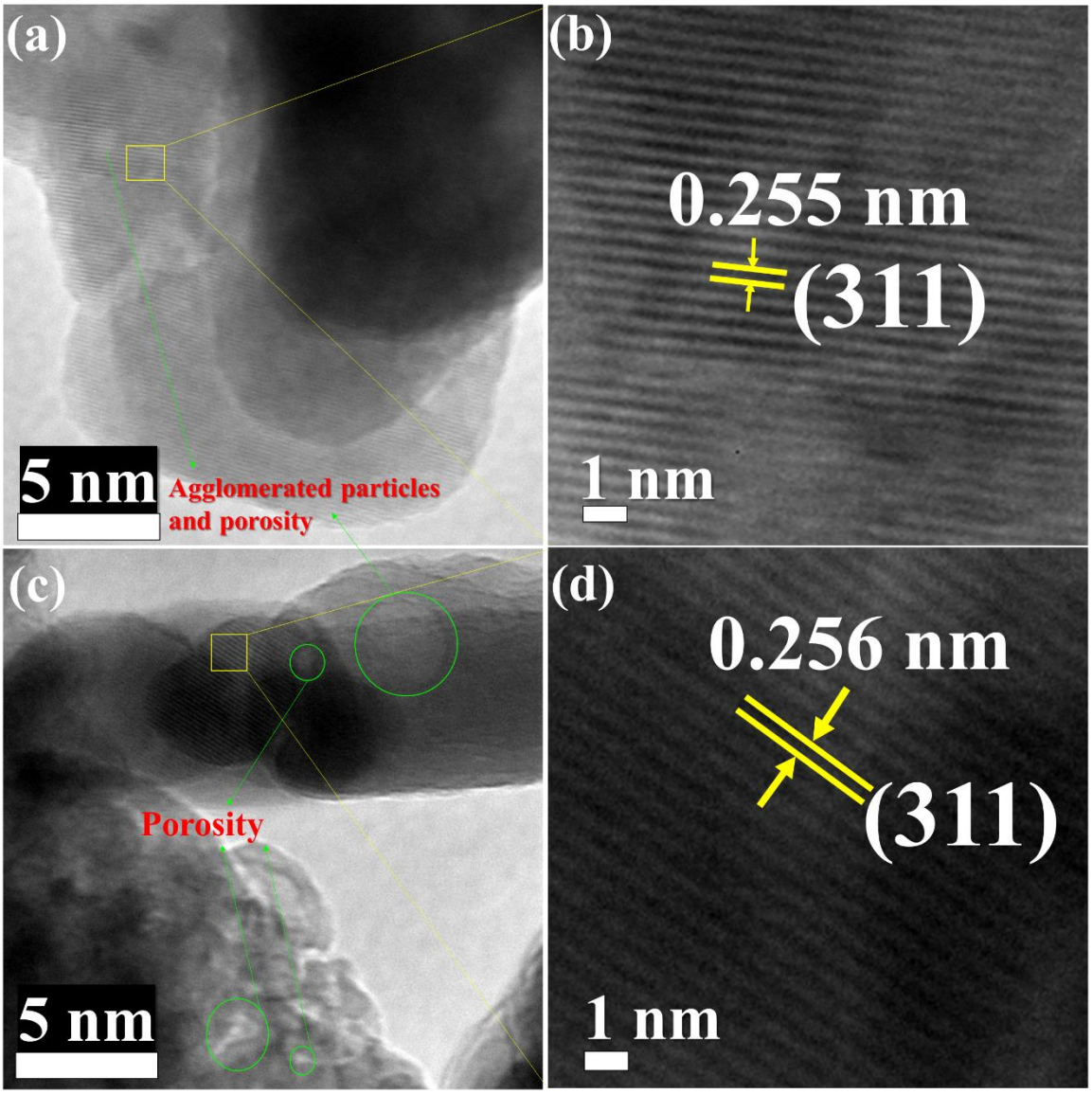

Fig. S4. HR-TEM image and enlarged lattice view of (a, b) CFVO, and (c, d) CZVO samples.

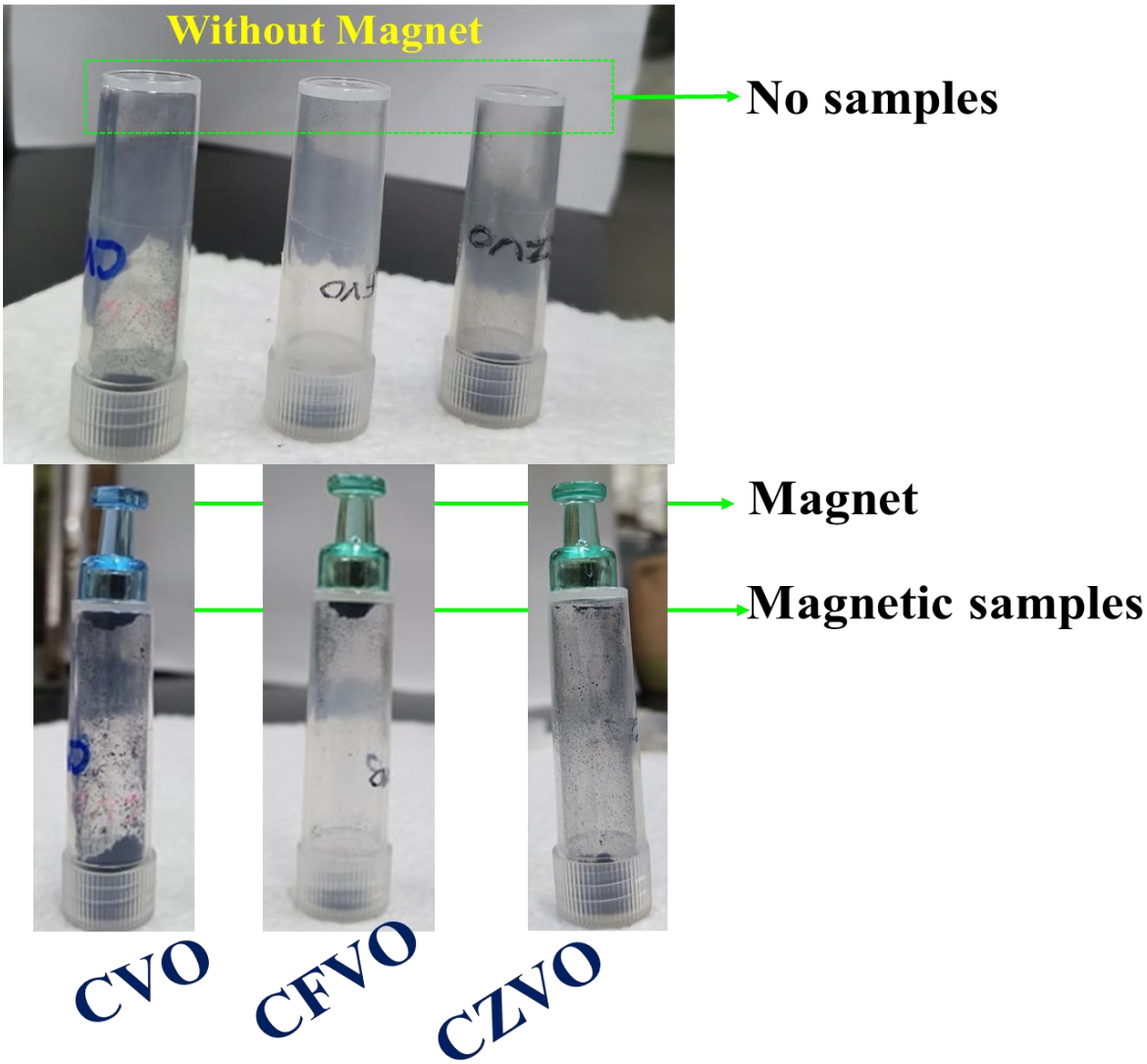

Fig. S5. Digital image of as-prepared materials with magnetic interaction.

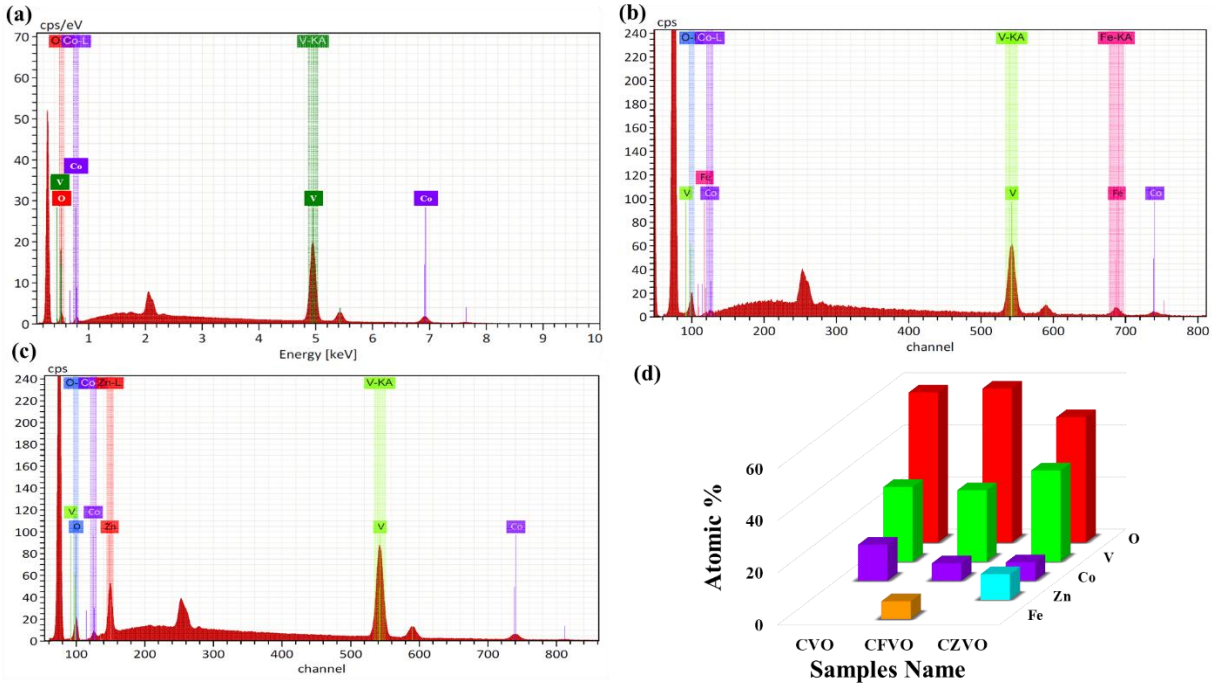

Fig. S6. SEM instrument coupled EDX spectra of **(a)** CoV_2O_4 (CVO), **(b)** $Co_{0.5}Fe_{0.5}V_2O_4$ (CFVO) and **(c)** $Co_{0.5}Zn_{0.5}V_2O_4$ (CZVO) materials.

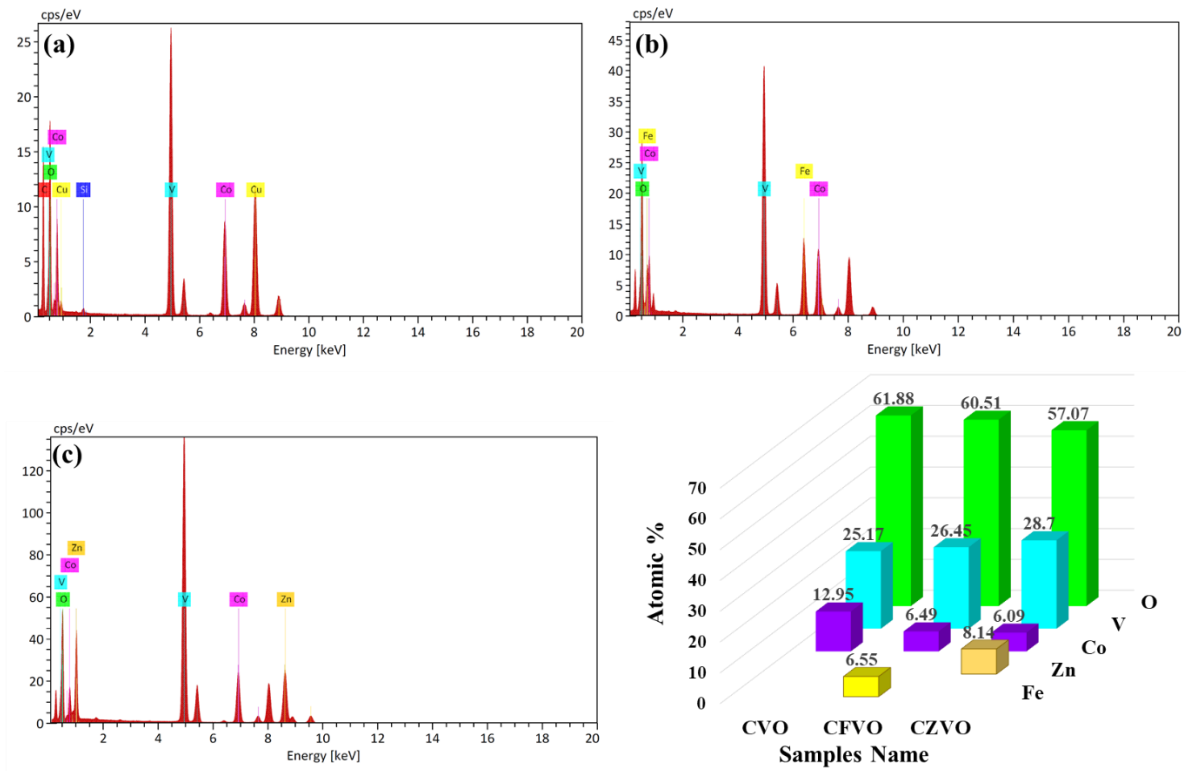

Fig. S7. TEM instrument coupled EDX spectra of (a) CoV_2O_4 (CVO), (b) $Co_{0.5}Fe_{0.5}V_2O_4$ (CFVO) and (c) $Co_{0.5}Zn_{0.5}V_2O_4$ (CZVO) materials.

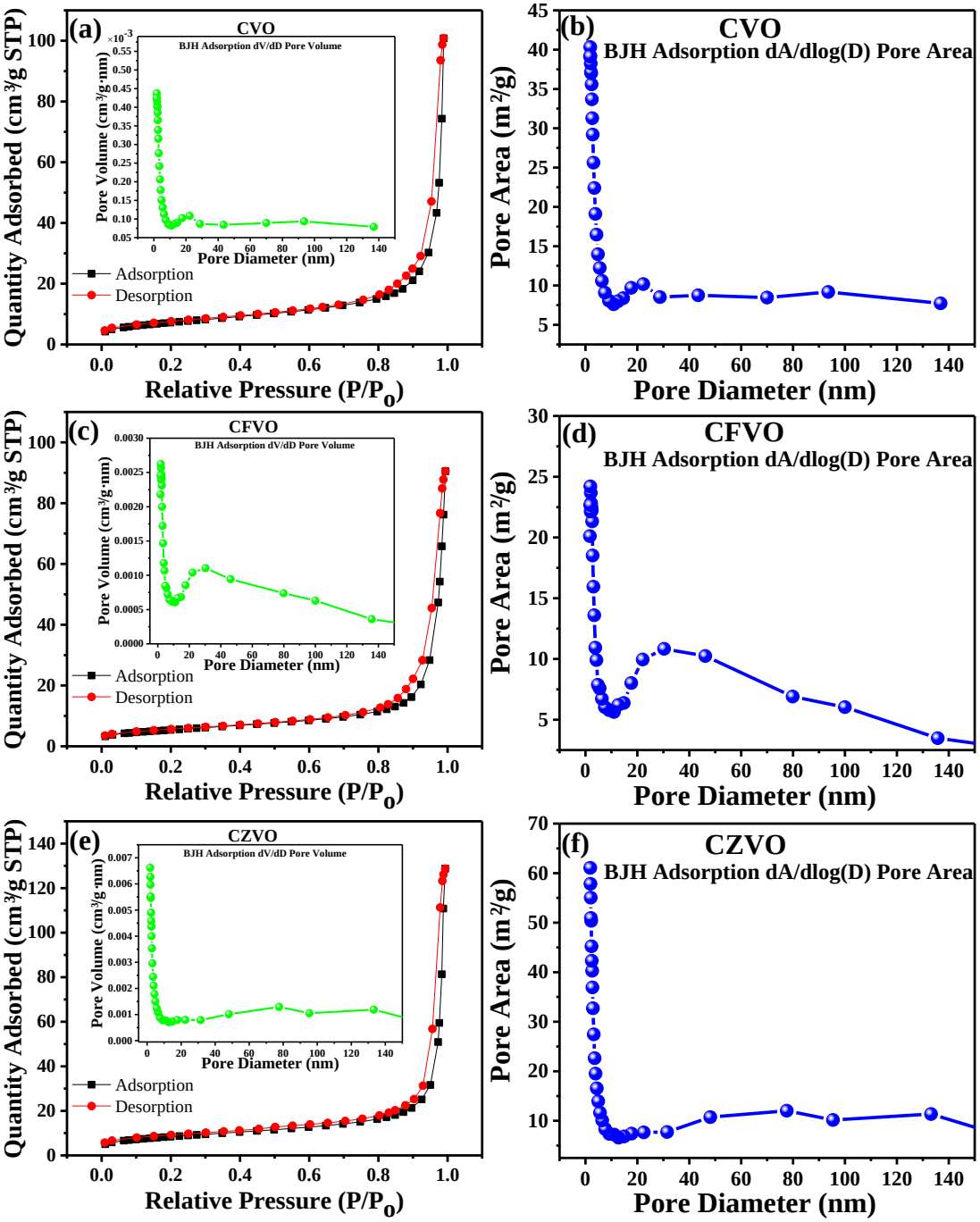

Fig. S8. (a, b) CoV_2O_4, **(c, d)** $Co_{0.5}Fe_{0.5}V_2O_4$ and **(e, f)** $Co_{0.5}Zn_{0.5}V_2O_4$ samples N_2 isotherm linear plots and their corresponding BJH pore size distributions analysis. The inset is pore volume versus pore diameter BJH absorption curve.

Table S3. The observed specific surface area and pore size distributions values from BET and BJH methods.

Samples	BET method		t-plot (Harkins and Jura method) micropore area (m^2/g)	Langmuir surface area (m^2/g)	BJH method	
	Specific surface area (m^2/g)	Average adsorption pore width (4V/A) (nm)			Cumulative adsorption pore volume diameter (cm^3/g)	average pore diameter (4V/A) (nm)
CVO	26.12	17.94	1.17	39.14	0.16	23.48
CFVO	19.19	24.57	0.98	29.40	0.14	27.90
CZVO	29.56	23.20	2.46	45.04	0.20	27.31

Electrochemical reaction Mechanism:

Ex-situ X-ray diffraction (XRD) was conducted to better realize the reaction mechanism of CoV_2O_4 (Fig.S9). During the lithiation (discharge) processes, the characteristics high intensity 2θ (~35.48°) and small intensity 2θ (~62.55°) diffraction peaks were gradually vanished with the deceasing of potential open circuit voltage (OCV) to 0.01V, representing the decomposition of crystalline CoV_2O_4. When completely discharged (at 0.01V) state, the broad peak was appeared at 42.2° with existing 2θ=45.6° new peak were attributed to the formation of metallic Co (ICSD# 44989) and V (ICSD# 43420), respectively. It is worth perceiving that the crystalline phase of CoV_2O_4 was not recovered after the initial charge. Similar, behaviour was reported in our work previous work[1] and other reports.[2,3]

Based on the *ex-situ* XRD results, the electrochemical reaction of CoV_2O_4 material can be suggesting the following reactions:[1]

$$CoV_2O_4 + 8Li^+ + 8e^- \rightarrow Co + 2V + 4Li_2O$$

$$Co + Li_2O \leftrightarrow CoO + 2Li^+ + 2e^-$$

$$2V + 3Li_2O \leftrightarrow V_2O_3 + 6Li^+ + 6e^-$$

For the increasing of the cyclic capacity during the prolonged cycle after the initial cycle, which may be the following reaction:[1]

$$CoO + 1/3Li_2O \leftrightarrow 1/3Co_3O_4 + 2/3Li^+ + 2/3e^-$$

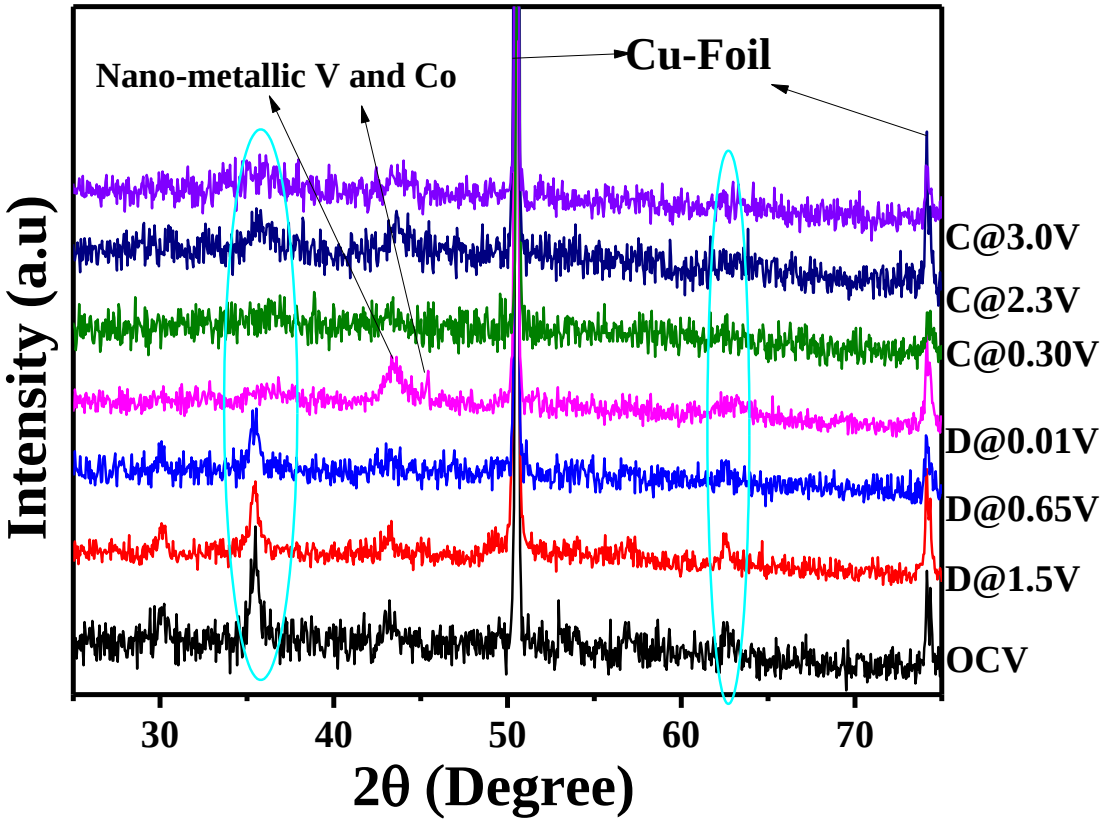

Fig. S9. *Ex-situ* XRD patterns of CoV_2O_4 electrodes at initial different discharge/charge states.

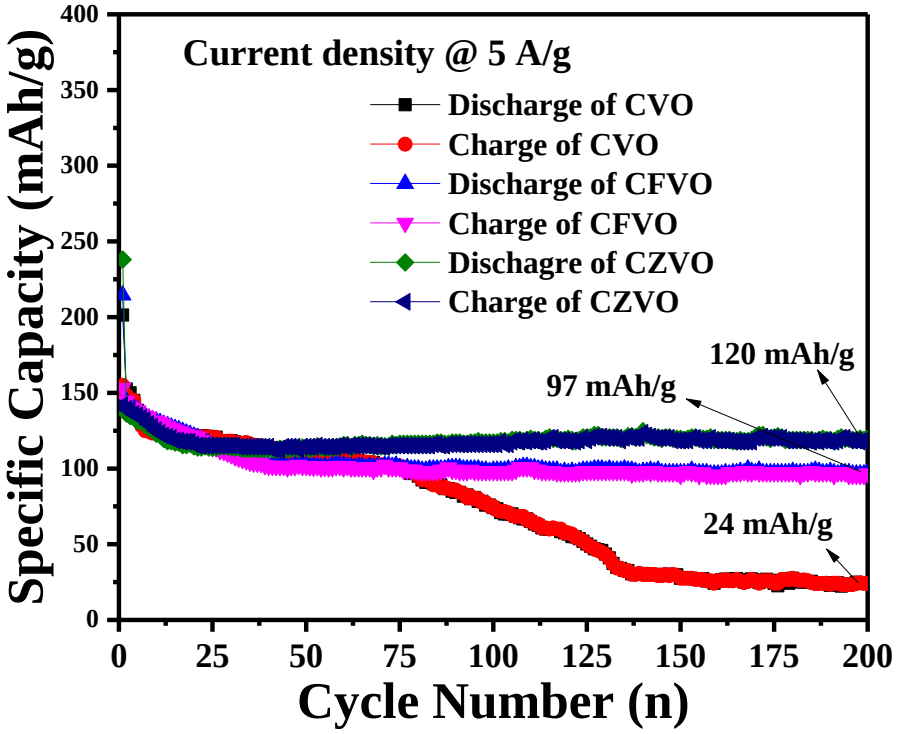

Fig. S10. High-rate long cyclic performance of CVO, CFVO and CZVO samples used cells at a current density of 5 A/g.

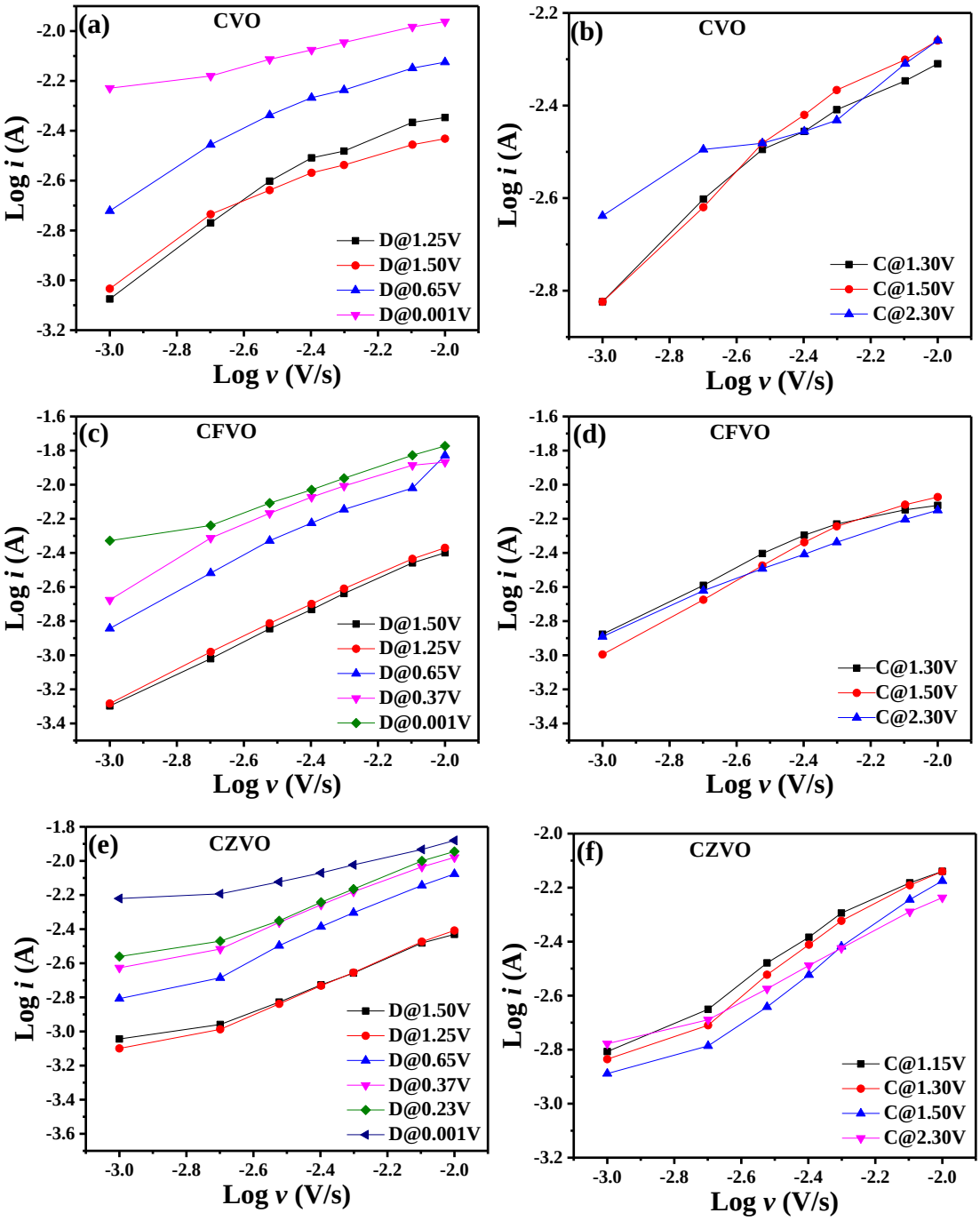

Fig. S11. Relationship between logarithm cathodic/anodic peak currents versus logarithm scan rates of **(a, b)** CVO, **(c, d)** CFVO, and **(e, f)** CZVO samples, respectively.

References

1. J. S. Lu, I. V. B. Maggay and W. R. Liu, CoV_2O_4: a novel anode material for lithium-ion batteries with excellent electrochemical performance, Chemical Communications, 2018, 54, 3094-3097.
2. S. Grugeon, S. Laruelle, L. Dupont and J. M. Tarascon, An update on the reactivity of nanoparticles Co-based compounds towards Li, Solid State Sciences, 2003, 5, 895-904.
3. X. Wang, Z. Jia, J. Zhang, X. Ou, B. zhang, J. Feng, F. Hou and J. Liang, Nanophase MnV_2O_4 particles as anode materials for lithium-ion batteries, Journal of Alloys and Compounds, 2020, DOI: https://doi.org/10.1016/j.jallcom.2020.156999, 156999.